Biomaterials Science

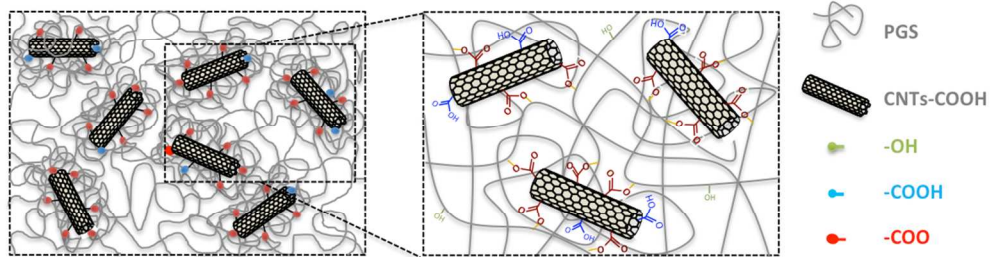# Elastomeric nanocomposite scaffolds made from poly (glycerol sebacate) chemically crosslinked with carbon nanotubes
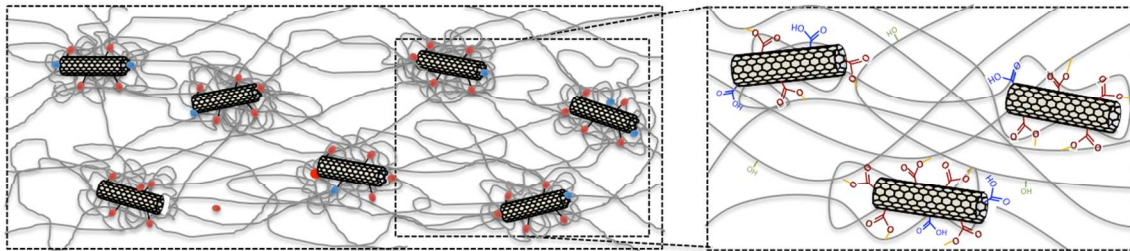
Table of contents

We report a general approach of fabricating stiff, elastomeric nanocomposites by covalent crosslinking poly(glycerol sebacate) (PGS) and CNTs for biomedical applications such as scaffolding in tissue engineering.

Biomaterials Science

ARTICLE

Elastomeric nanocomposite scaffolds made from poly (glycerol sebacate) chemically crosslinked with carbon nanotubes

Akhilesh K. Gaharwar[a,b,x,$,‡,*], Alpesh Patel[c,d,‡], Alireza Dolatshahi-Pirouz[b,c,d,α], Hongbin Zhang[c,d], Kaushik Rangarajan[c,d], Giorgio Iviglia[c,d], Su-Ryon Shin[b,c,d], Mohammad Asif Hussain[e], Ali Khademhosseini[b,c,d,f,g,*]

Carbon nanotube (CNT)-based nanocomposites often possess properties such as high stiffness, electrical conductivity, and thermal stability and have been studied for various biomedical and biotechnological applications. However, the current design approaches utilize CNTs as physical filler, and thus, the true potential of CNT-based nanocomposites has not been achieved. Here, we introduce a general approach of fabricating stiff, elastomeric nanocomposites from poly(glycerol sebacate) (PGS) and CNTs. The covalent crosslinking between the nanotubes and polymer chains resulted in novel property combinations that are not observed in conventional nanocomposites. The addition of 1% CNTs resulted a five-fold increase in the tensile modulus and a six-fold increase in compression modulus compared with PGS alone, which is far superior to the previously reported studies for CNT-based nanocomposites. Despite significant increase in mechanical stiffness, the elasticity of the network was not compromised and the resulting nanocomposites showed more than 94% recovery. This study demonstrates that the chemical conjugation of CNTs to a PGS backbone results in stiff and elastomeric nanocomposites. Additionally, *in vitro* studies using human mesenchymal stem cells (hMSCs) indicated that the incorporation of CNTs to PGS network significantly enhanced the differentiation potential of the seeded hMSCs rendering them potentially suitable for applications ranging from scaffolding in musculoskeletal tissue engineering to biosensors in biomedical devices.

Introduction

Carbon nanotubes (CNTs) have shown exceptional structural, electrical, mechanical, and thermal properties.[1-3] CNTs-based nanocomposites possess unique property combinations and have been explored for numerous technological applications such as actuators,[4, 5] body armor,[6] conductive tapes,[7] flame retardant,[8] energy storage,[9] tissue engineering,[10, 11] delivery devices,[12, 13] biosensors,[14-16] and biomedical devices.[17-19] Despite interesting physical and chemical properties, the true potential of CNTs-based nanocomposites has yet to be realized.[20-22] This is due to strong π-π stacking interactions between CNTs that limits the dispersion of CNTs within polymeric matrix and decreases its ability to improve the structural, chemical and biological properties of the nanocomposites network.

To overcome this shortcoming, numerous techniques are used to augment the dispersion of CNTs within the polymeric network such as surface functionalization.[23-26] The surface of CNTs are modified with different polar groups including carboxyl,[27] hydroxyl,[28] and amine,[29] to facilitate their uniform distribution within polymeric matrix. Other strategies to enhance solubility of CNTs in aqueous and non-aqueous solutions include the use of surfactants,[30] proteins,[31] and single-stranded deoxyribonucleic acid (ssDNA)[32]. The uniform dispersion of CNTs within the polymeric network results in enhanced surface interactions and significant increases in stiffness of the nanocomposites.[33]

Grafting polymeric chains on nanotube surfaces can modify the surface of CNTs.[34] In this approach, polymeric chains shield the surface of CNTs and the adjoining polymeric network simply recognizes the surface-grafted polymer. This shielding method improves CNTs distribution within the polymeric matrix due to increase in physical interactions between polymer chains and surface-grafted CNTs. Two different strategies that are currently employed to covalently graft polymers on CNTs surfaces are "grafting from" and "grafting to." The "grafting to" strategy showed limitations in obtaining dense grafting density on the CNTs surfaces due to the steric hindrance of reactive groups presence on the polymer backbone and a relatively small number of functional groups available on the surface of CNTs. However, the "grafting from" strategy showed the formation of dense grafting of polymers on the CNTs surfaces. During the last decade, these strategies were

extensively used to physically reinforce polymeric networks with CNTs to obtain mechanically superior nanocomposites.[21, 22] In a recent study, the CNT surfaces were grafted with poly(cyclohexyl methacrylate) using surface-initiated atom transfer radical polymerization. The grafting of polymer on CNTs significantly enhanced the electrical and mechanical properties of resultant nanocomposites.[35]

Despite the increase in interaction between CNTs and polymeric network, the utility of CNTs as a reinforcing agent has yet to be fully exploited as most studies have used functionalized CNTs as physical reinforcer.[29-27] By chemically conjugated CNTs surfaces with the polymeric network, CNTs can be used as a crosslinking agent. To our knowledge, limited efforts are directed towards utilizing CNTs as a crosslinking agent. It is expected that if CNTs are covalently conjugated within the polymeric network, novel property combinations may be achieved.

To design CNTs-reinforced composite, poly(glycerol sebacate) (PGS)[36, 37], a polyester, is selected to chemically conjugate with CNTs. PGS is an elastomeric polyester synthesized by polycondensation of sebacic acid and glycerol without the presence of any toxic catalyst.[37] The availability of additional hydroxyl groups hydrates the PGS surface and provides a tissue-like environment to cells. Due to the elastomeric property of PGS, it has been used to engineer soft tissues such as cardiac, renal, and heart valve tissues.[38, 39] When implanted *in vivo*, PGS is readily metabolized under physiological conditions since both glycerol and sebacic acid, are endogenous components. Moreover, the degradation of PGS follows the surface erosion mechanism and can be tailored to follow the ECM biosynthesis without exhibiting any sudden change in structural, physical and chemical properties.[37]

Here, we developed chemically crosslinked PGS-carbon nanotube (PGS-CNT) nanocomposites. The additional hydroxyl groups present on PGS backbone esterify with the carboxylic groups present on CNTs surfaces during the thermal curing process, which is an advantage over other polyester-based nanocomposites. The chemical conjugation of CNTs with polyester backbone considerably amplifies the physical and chemical properties of the nanocomposites. By covalently conjugating PGS with CNTs, we expect to obtain mechanically stiff nanocomposites that can be used for a range of biomedical applications, including as bone scaffolds, cardiac patches, nerve conduits, as well as for a range of other biomedical devices.

Materials and methods

Synthesis of poly(glycerol sebacate) (PGS)

Sebacic acid (M_w=202.25 g/mol, $HO_2C(CH_2)_8CO_2H$), and glycerol (M_w=92.09 g/mol, $HOCH_2CH(OH)CH_2OH$) was obtained from Sigma-Aldrich (USA). PGS was synthesized by polycondensation reaction using previously reported method.[39, 40] Briefly, glycerol and sebacic acid (1:1 molar ratio) were mixed in a 250 mL two necks round bottom flask and heated to 130°C in a silicon bath (under argon blanket for 2 hours). The pressure was then decreased to 50 mTorr in 5 hours, and the reaction was continued for 24 hours at 130°C. The PGS prepolymer solution was then cooled to room temperature and its molecular weight distribution was analyzed using gel permeation chromatography (GPC) (M_n=3960 g/mol; PDI=1.6). Since, the initial molar ratio of carboxylic acid to hydroxyl groups was 2:3, additional hydroxyl groups were available on PGS backbone for further crosslinking.

Synthesis of PGS-CNTs nanocomposites

Carboxyl functionalized multi-walled CNTs (50–250 μm in length; ~9±8 nm in diameter; 95% purity) were obtained from NanoLab Inc. (MA, USA). The nanocomposites were prepared by mixing PGS prepolymer in tetrahydrofuran (THF) (50% w/v) and adding a specific amount of CNTs (0.25, 0.5, and 1%) to the solution. CNTs were suspended in the PGS solution using ultrasonication. A substantial increase in the viscosity of PGS solution was detected due to strong interactions between PGS and CNTs. The solution was then poured in Teflon-based flat petri dish and the THF was evaporated overnight. The obtained films were cured at 130°C for 40 hours under vacuum. The nanocomposites were named as PGS-0.25%CNTs, PGS-0.5%CNTs and PGS-1%CNTs respectively depending on the final concentration of CNTs with respect to PGS.

Chemical characterizations

An Alpha FTIR Bruker spectrometer was used to determine Fourier Transform Infrared (FTIR) spectra of the samples. 48 scans at a resolution of 4 cm^{-1} were obtained for each sample. Raman spectra of the samples were recorded using a R200-L SENTERRA Raman microscope on Olympus BX51 microscope stand using excitation: 785nm and 532 nm (He–Ne laser, with a power of 5 mW as the excitation source). The optical spectra of the samples were measured using an UV/vis spectrophotometer (Epoch Biotech Instruments).

Sol content analysis

The crosslinking degree of nanocomposite network was evaluated by determining sol (uncrosslinked polymer or nanotubes) and gel (crosslinked network) contents. The nanocomposite samples (8 mm diameter and 2 mm thick, and initial weight (W_i)) were swollen in THF for 24 hours (n=5) (swollen weight (W_s)). The swollen samples were washed with THF and dried overnight (final weight (W_d)). The percentage of sol contents and degree of swelling were calculated by

$$Sol\ (\%) = \frac{(W_i - W_d)}{W_i} \times 100 \qquad \text{Eq. (1)}$$

$$Degree\ of\ swelling\ (\%) = \frac{(W_s - W_d)}{W_s} \times 100 \qquad \text{Eq. (2)}$$

Thermal analysis

The thermal properties of nanocomposite network were investigated using differential scanning calorimetry (DSC) (DSC8500, Perkin-Elmer, USA) and thermogravimetry analysis (TGA) (Pyris 1 TGA, Perkin-Elmer, USA). The samples were dried at 35°C overnight under vacuum. For TGA, samples (~10 mg) were subjected to a heating cycle of 50°C to 600°C at 10°C/min heating rate. Initial degradation temperature (T_{DI}) and peak degradation temperature (T_{DP}) was determined using first derivative curve to determine the onset of thermal degradation. For DSC, samples (~3-5 mg) were heated from -70°C to 100°C under N_2 at the rate of 10°C/min, held at 100°C for 5 min, and cooled down to -70°C at the rate of 10°C/min. The 1st cooling cycles and 2nd heating cycles were used to determine the thermal properties (glass transition temperature (T_g), melting point (T_m), enthalpy of the composites (ΔH)). Considering the thermal decomposition as first-order reaction, the activation energy (E_a) was calculated using the Horowitz-Metzger method[41, 42] as shown in Eq. (3):

$$ln\left(ln\left(^1/_y\right)\right) = {-E_a\theta}/{RT_d^2} \qquad \text{Eq. (3)}$$

Here, E_a is activation energy (kJ/mol); y is the weight loss in fraction; T_d is reference temperature ($^\circ k$), R is the universal gas constant and $\theta = (T - T_d)$ ($^o k$). The slope obtained from linear plots of $ln\left(ln\left(^1/_y\right)\right)$ vs θ was used to calculate the activation energy.

Mechanical analysis

The mechanical properties of nanocomposite samples were evaluated using uniaxial tensile, and unconfined compression testing using Instron 5943 Materials Testing System (Norwood, MA, USA) loaded with 50 N load cell. For uniaxial tensile, nanocomposite samples (2mm wide, 5 mm long x 1.5 mm thick) were used. For compression testing, nanocomposite samples with 5mm diameter, and 2 mm thick were used. The crosshead speed of 10 mm/min was used for both tensile and compression testing. For cyclic testing, 5 cycles consisting of a loading and an unloading cycle were implemented. The maximum strain was limited to 20%. Mechanical properties such as compressive modulus, ultimate compressive stress, ultimate compressive strain, toughness, and energy absorbed were calculated from the stress-strain curve. The elastic modulus was determined from the linear stress-strain region by fitting a straight line between 5 to 20 % strain.

Scanning electron microscopy

The structural morphologies of the nanocomposite surface were evaluated using a scanning electron microscope (JSM 5600LV, JEOL USA Inc., MA). The samples were freeze-fractured using liquid nitrogen to visualize the distribution of CNTs within the PGS network. The samples were allowed to dry in a desiccator for 24 hours before imaging. The nanocomposite samples were coated with Au/Pd for 2 minutes using a Hummer 6.2 sputter coater (Ladd Research, Williston, VT). The fractured surfaces of the nanocomposite samples from the mechanical testing were also analyzed using this method.

Surface analysis, swelling and degradation study

The surface hydrophilicity of nanocomposite films (n=5) was determined using drop shape analysis method. A drop of water was poured on the nanocomposite surface using 21-gauge flat needle and optical images were collected after 10 second of contact. The contact angle of water was determined from the optical images. The swelling degree and degradation of nanocomposite samples (6mm diameter, 2mm thick and dried weight (W_i)) were determined in phosphate buffer saline (PBS) at 37°C. For swelling study, samples were collected after 24 hours, blotted the excess surface water and weighed (W_s). The water-swelling ratio was calculated using Eq. (2). For degradation study, sample at predetermined time were obtained from PBS, and dried weight (W_d) was determined. The related mass losses were calculated from Eq. (4) from their initial and final dry weight.

$$Degradation\,(\%) = \frac{(W_i - W_d)}{W_i} \times 100 \qquad \text{Eq. (4)}$$

Protein adsorption

The adsorption of protein on nanocomposite surface was determined by soaking the samples (6 mm diameter and 2mm thick) in PBS overnight and then in 10% fetal bovine serum (FBS) for 24 hours at 37 °C. The samples were washed three times with PBS for 10 minutes to remove non-specifically adsorbed proteins. Then samples were subjected to 2% sodium dodecyl sulfate (SDS) solution under shaking conditions (50 rpm, 37°C) for 6 hours to collect adhered proteins. The supernatant was collected and analyzed using bicinchoninic acid (BCA) protein assay reagent (Pierce BCA, Thermo Scientific). The bovine serum albumin was used as standard and the supernatant was quantified using an UV/vis spectrophotometer (Epoch Biotech Instruments) at 562 nm.

In vitro **study**

Bone marrow-derived hMSCs (PT-2501, Lonza, USA) were cultured in normal growth media (α-MEM, containing 10% of heat-inactivated fetal bovine serum (HiFBS, Gibco, USA) and 1% Pen/Strep (penicillin/streptomycin, 100U / 100 µg/mL, Gibco, USA) at 37°C, in a humidified atmosphere with 5% CO_2. Before cell seeding, the nanocomposite scaffolds were washed using 80-90% ethanol solution and subjected to UV light, followed by thorough washing with PBS. The cells were cultured until 70-75% confluence and were used before passage 4 for all the experiments. The cells were trypsinized (CC-3232, Lonza, USA) and seeded on nanocomposite scaffolds (6 mm cylindrical samples) at the density of 10,000 cells/sample in normal growth media. Cell proliferation over 7 days of culture was evaluated using Alamar Blue Assay (Invitrogen, USA) following the standard manufacturer protocol. For osteogenic differentiation studies, osteogenic media (PT-3924 & PT-4120, Lonza, USA) supplemented with Pen/Strep, L-glutamine, ascorbate, β- glycerolphosphate, and dexamethasone was used. Alkaline phosphatase (ALP) activity of hMSCs seeded on the nanocomposite surface was quantified on days 7, 14 and 21 using ALP Colorimetric Assay Kit (ab83369 Abcam, USA) following the standard manufacturer protocol. The amount of calcium was quantified using Calcium Quantification Assay kit (ab112115 Abcam, USA) following the standard manufacturer protocol. The ALP activity and calcium content from each sample was normalized to the DNA content with a Quant-iT PicoGreen kit (Invitrogen, USA) following the standard manufacturer protocol.

Statistics

The experimental results are represented as mean ± standard deviation (n=3 to 5). One-way ANOVA with Tukey post-hoc analysis was used to determine the statistical differences between the groups for fiber analysis, mechanical testing and drug loading, while two-way ANOVA was used for ALP analysis. Statistical significance was represented as *p<0.05, **p<0.01, ***p<0.001.

Results and discussion

Covalently reinforced PGS-CNTs nanocomposites

The covalently reinforced PGS-CNTs nanocomposites were obtained by a two-step process. In the first step, a low molecular weight PGS prepolymer (M_n= 3960 gm/mol and PDI = 1.6) was prepared by polycondensation method. Then the PGS prepolymer was dissolved in THF (50% w/v) and the carboxylic functionalized CNTs were incorporated in the PGS prepolymer solution using ultrasonication. The covalently reinforced PGS-CNTs nanocomposites obtained by a two-step process exhibited an increased solution viscosity solution during the process. This implies that low molecular weight PGS

prepolymer strongly interacts with carboxyl functionalized CNTs. The resulting PGS-CNTs solution was found to be stable with no phase separation or segregation. This PGS-CNTs prepolymer mixture was then allowed to dry in a vacuum to evaporate the solvent (THF). In the second step, dried PGS-CNTs prepolymer film was subjected to 130°C for 40 hours to obtain covalently crosslinked PGS-CNTs nanocomposites (Figure 1a). During this curing step, hydroxyl groups that are present on the PGS chains esterifies with the carboxyl groups present on the CNTs surface to form a covalently crosslinked network.

The optical images indicate uniform distribution of CNTs within the PGS network. As the concentration of CNTs increases, the transparency (Figure 1b) of the nanocomposite film decreases. This is also evident by the increase in absorbance value in the visible spectra (400-700 cm^{-1}). At macroscopic length scale, uniform dispersion of CNTs within the PGS matrix was observed. The dispersion of CNTs at micro- and nano-length scale was observed using electron microscopy. The electron microscopy images of fractured nanocomposite surface (Figure 1c) indicate uniform distribution of CNTs within a polymeric matrix. All the nanocomposite

films show high flexibility and can sustain bending and twisting (Figure 1d).

The Raman spectra of the PGS-CNTs nanocomposites were obtained to determine the interactions between PGS and CNTs (Figure 1e). The Raman spectra of multiwall CNTs display two characteristic peaks – 1580 cm^{-1} (Graphite or G-band) and 1360 cm^{-1} (distorted or D-band). The G-band derives from the graphite-like in-plane mode (also known as tangential mode), whereas D-band corresponds to intrinsic impurities or defects of nanotubes. For carboxylic functionalized CNTs, G-band is stronger compared to D-band. After thermal crosslinking of PGS with CNTs, the intensity of D-band was greater than G-band. This indicates that the structure of CNTs was distorted due to chemical conjugation of CNTs with PGS chains. Earlier studies have also showed that covalent conjugation of polymer to CNT surfaces result in an increase in D-band intensity.[43, 44] The infrared spectra (IR) also indicated fabrication of chemically crosslinked nanocomposite network after the thermal crosslinking process. The peaks at 1350 cm^{-1} (-COOH), 1100 cm^{-1} (-OH) and 3450 cm^{-1} (-OH) decreased after the crosslinking process (Figure 1f). The addition of 1% CNTs further resulted in the reduction of these peaks, indicating higher degree of crosslinking compared to pure PGS.
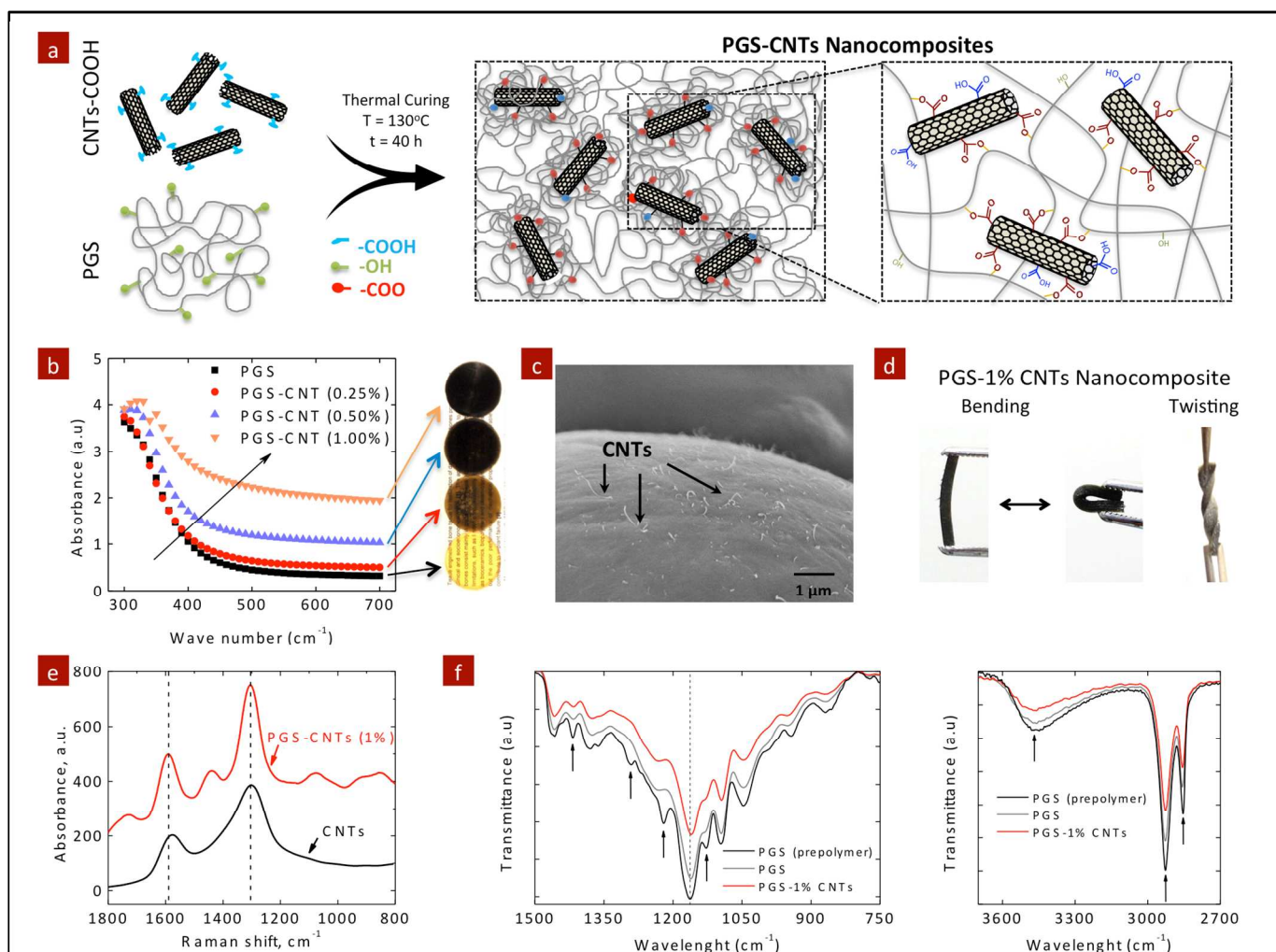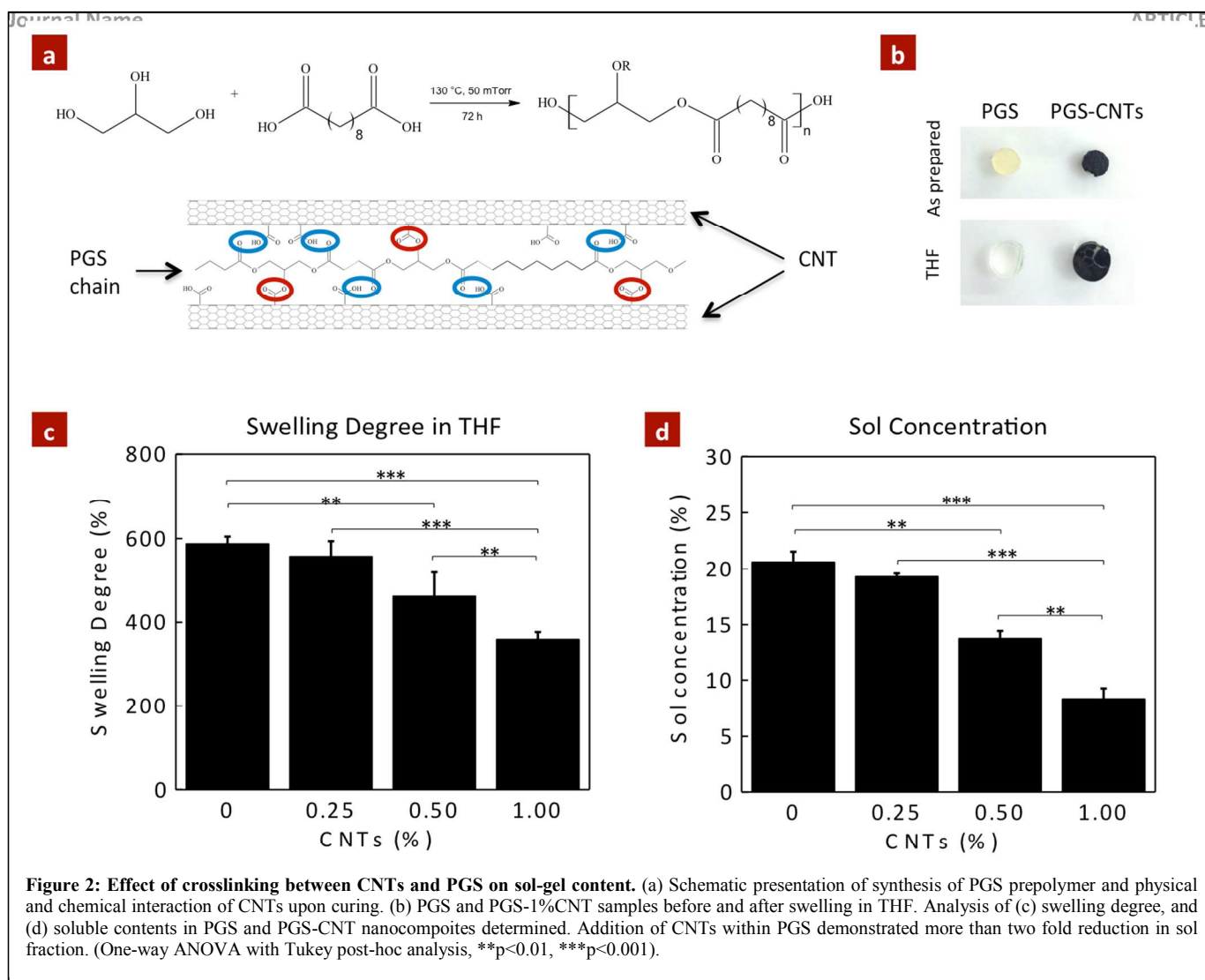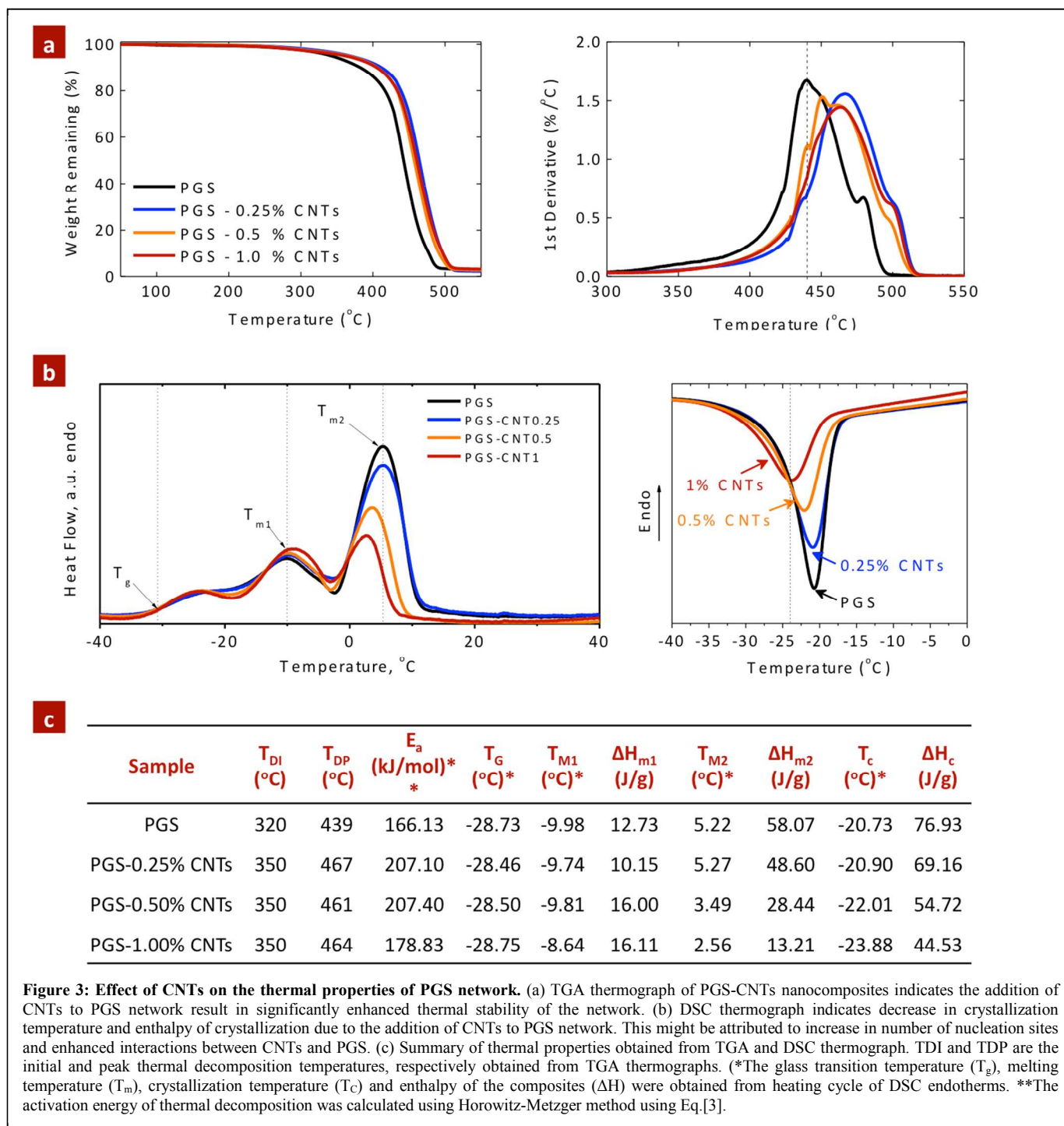

Figure: 1 Synthesis and fabrication of PGS-CNTs nanocomposites. (a) Schematic representation of PGS-CNT nanocomposite synthesis. COOH-functionalized CNTs act as both physical and covalent crosslinker. The presence of hydroxyl groups on PGS backbone esterifies with the carboxylic groups present on CNTs surfaces during the thermal curing process, resulting in densely crosslinked network. (b) UV-vis spectra of PGS-CNT nanocomposites showing decrease in optical transmittance due to addition of CNTs. (c) SEM image of freeze-fractured surface of PGS-1% CNTs nanocomposite show uniform distribution of CNTs on the surface. (d) PGS-CNTs nanocomposites show high flexibility and can sustain bending and twisting. (e) Raman spectra of CNT and PGS-CNT nanocomposites. The COOH- functionalized CNTs, show a stronger G-band compared to D-band. After thermal crosslinking of PGS with CNTs, the intensity of D-band was greater than G-band. This indicates that the structure of CNTs was distorted due to chemical conjugation of CNTs with PGS chains. (f) FTIR spectra of PGS-CNTs nanocomposites. Reduction in hydroxyl peak up on curing in presence of CNTs supports the covalent interaction of CNTs within PGS network.

Journal Name   ARTICLE

Figure 2: Effect of crosslinking between CNTs and PGS on sol-gel content. (a) Schematic presentation of synthesis of PGS prepolymer and physical and chemical interaction of CNTs upon curing. (b) PGS and PGS-1%CNT samples before and after swelling in THF. Analysis of (c) swelling degree, and (d) soluble contents in PGS and PGS-CNT nanocompoites determined. Addition of CNTs within PGS demonstrated more than two fold reduction in sol fraction. (One-way ANOVA with Tukey post-hoc analysis, **p<0.01, ***p<0.001).

Another method to ascertain the covalent crosslinking between PGS and CNTs is to determine the change in crosslinking density due to the addition of CNTs. The crosslinking density of the nanocomposites network was determined by evaluating the amount of sol content (uncrosslinking macromer) within the network. It is expected that the esterification of CNTs with excess hydroxyl groups available on the PGS backbone provides additional crosslinking sites, and significantly reduces the amount of sol content (Figure 2a). The amount of sol within the nanocomposites was determined using THF. PGS readily swells in THF, and thus the sol can be easily leached out and the amount of gel (crosslinked network) can be determined (Figure 2b). The addition of CNTs to PGS network result in lower swelling degree in THF (Figure 2c). For example, pure PGS swells to 987±17%, whereas the addition of 0.25, 0.5 and 1% CNTs reduces the swelling degree to 557±36%, 462±56% and 357±20% respectively (Figure 2c). The amount of sol for PGS was determined to be 20.63±0.67%, similar to the previously reported literature.[45] The addition of CNTs as a chemical crosslinker significantly decreases the amount of sol content due to enhanced crosslinking between CNTs and PGS (Figure 2d). The sol content for PGS nanocomposites containing 0.25, 0.5, and 1% CNTs were 19.33±0.19%, 13.67±0.86%, and 8.36±0.77%, respectively. The addition of 1% CNTs reduces the sol content by 60% to that of pure PGS. These results indicate that CNTs acted as a multifunctional crosslinker and covalently crosslinked with PGS chains.

Thermal stability of PGS-CNTs nanocomposites

Sample	T_{DI} (°C)	T_{DP} (°C)	E_a (kJ/mol)**	T_G (°C)*	T_{M1} (°C)*	ΔH_{m1} (J/g)	T_{M2} (°C)*	ΔH_{m2} (J/g)	T_c (°C)*	ΔH_c (J/g)
PGS	320	439	166.13	-28.73	-9.98	12.73	5.22	58.07	-20.73	76.93
PGS-0.25% CNTs	350	467	207.10	-28.46	-9.74	10.15	5.27	48.60	-20.90	69.16
PGS-0.50% CNTs	350	461	207.40	-28.50	-9.81	16.00	3.49	28.44	-22.01	54.72
PGS-1.00% CNTs	350	464	178.83	-28.75	-8.64	16.11	2.56	13.21	-23.88	44.53

Figure 3: Effect of CNTs on the thermal properties of PGS network. (a) TGA thermograph of PGS-CNTs nanocomposites indicates the addition of CNTs to PGS network result in significantly enhanced thermal stability of the network. (b) DSC thermograph indicates decrease in crystallization temperature and enthalpy of crystallization due to the addition of CNTs to PGS network. This might be attributed to increase in number of nucleation sites and enhanced interactions between CNTs and PGS. (c) Summary of thermal properties obtained from TGA and DSC thermograph. TDI and TDP are the initial and peak thermal decomposition temperatures, respectively obtained from TGA thermographs. (*The glass transition temperature (T_g), melting temperature (T_m), crystallization temperature (T_C) and enthalpy of the composites (ΔH) were obtained from heating cycle of DSC endotherms. **The activation energy of thermal decomposition was calculated using Horowitz-Metzger method using Eq.[3].

The chemical infusion of CNTs within the PGS network had improved thermal stability compared to the pure PGS network. The weight loss characteristic of PGS and PGS-CNTs nanocomposites was evaluated using thermal gravimetric analysis (TGA) (Figure 3a). The derivative curve of the thermal decomposition spectra of PGS and PGS-CNTs nanocomposites indicate a multiple-steps degradation profile. These steps are introduced due to the polydispersity of the PGS macromer. First derivative curve, used to evaluate the initial degradation temperature (T_{DI}), indicates onset of degradation and the peak degradation temperature (T_{DP}). For PGS, T_{DI} was ~320°C and

T_{DP} was ~439°C (Figure 3a). The infusion of CNTs (0.25%) within the PGS network enhances the thermal stability of nanocomposites (T_{DI} ~350°C and T_{DP}~467°C) due to strong covalent interactions between CNTs with PGS. Improved thermal stability of the nanocomposites was attributed to covalent crosslinking between CNTs and PGS that constrains segmental motion of PGS backbone. However, no effect on T_{DI} and T_{DP} was observed due to a further increase in CNTs. Similar trends of improving the thermal stability of polymers after reinforcing with CNTs were reported previously.[46, 47] The effect of CNT addition on the kinetics of thermal

decomposition of the nanocomposite network was also investigated. The activation energy of PGS and PGS-CNTs nanocomposites was shown in Figure 3c. The addition of CNTs to PGS results in an increase in activation energy and the data implied uniform dispersion of CNTs within the PGS network.

The effect of CNTs on phase transformation of PGS was investigated using DSC. As shown in DSC endotherms (Figure 3b), the glass transition temperature (T_g) of PGS was observed around -28.5°C. A weak endothermic peak at -10°C (T_{m1}) followed by a strong endothermic peak at 5.5°C (T_{m2}) were due to the melting points of PGS, similar to previously reported literature.[48] The addition of CNTs had no effect on T_g, however, the melting points were decreased due to the disruption of the polymeric network by CNTs. During the cooling cycle, an exothermic crystalline peak was observed in PGS, similar to previously reported literature.[39] As shown in the cooling cycle, the presence of CNTs within PGS network decreases both the crystallization temperature and the enthalpy of crystallization (Figure 3c). The addition of CNTs increases the number of nucleation sites and the strong interactions between CNTs and PGS results in decrease in crystallization degree and the enthalpy of recrystallization. Similar results were reported by Liang *et al.* on PGS-bioglass composites.[49] They reported a decrease in recrystallization energies and recrystallization temperature due to the addition of bioglass to the PGS network. Overall, the results indicate that PGS-CNTs nanocomposites are semicrystalline elastomers below their

melting point, and amorphous at the physiological temperature.

Mechanical properties of PGS-CNTs nanocomposites

The covalent crosslinking of PGS and CNTs significantly improved the mechanical properties of the polymeric network. Due to covalent crosslinking of CNTs within PGS network, it is expected that higher load is required to deform the network compared to pure PGS network (Figure 4a). The mechanical stiffness of PGS-CNTs nanocomposites was evaluated using uniaxial tensile testing (Figure 4b). The elastic modulus and ultimate tensile strength (UTS) of pure PGS was 198±20 kPa and 122±16 kPa, respectively. The addition of CNTs (up to 1%) to PGS resulted in more than a two-fold increase in UTS (275±44 kPa) and in more than a five-fold enhancement in tensile modulus compared to PGS network (Figure 4c). For example, the nanocomposites containing 0.25, 0.5, and 1% of CNTs resulted in an increase in elastic modulus to 287±13, 732±77, and 1014±103 kPa, respectively. While, the addition of CNTs to the PGS network resulted in decrease in the total elongation of nanocomposites pure PGS showed maximum elongation of 122±15%. The addition of 0.25, 0.5, and 1% CNTs reduced elongation to 99±10, 38±4, and 43±5%, respectively. The decrease in elongation is expected due to an increase in crosslinking density with an addition of CNTs. We further analyzed the fracture mode of the nanocomposites using electron microscopy (Figure 4d). PGS generated an elastomeric scaffold and the fractured surface of PGS indicates the
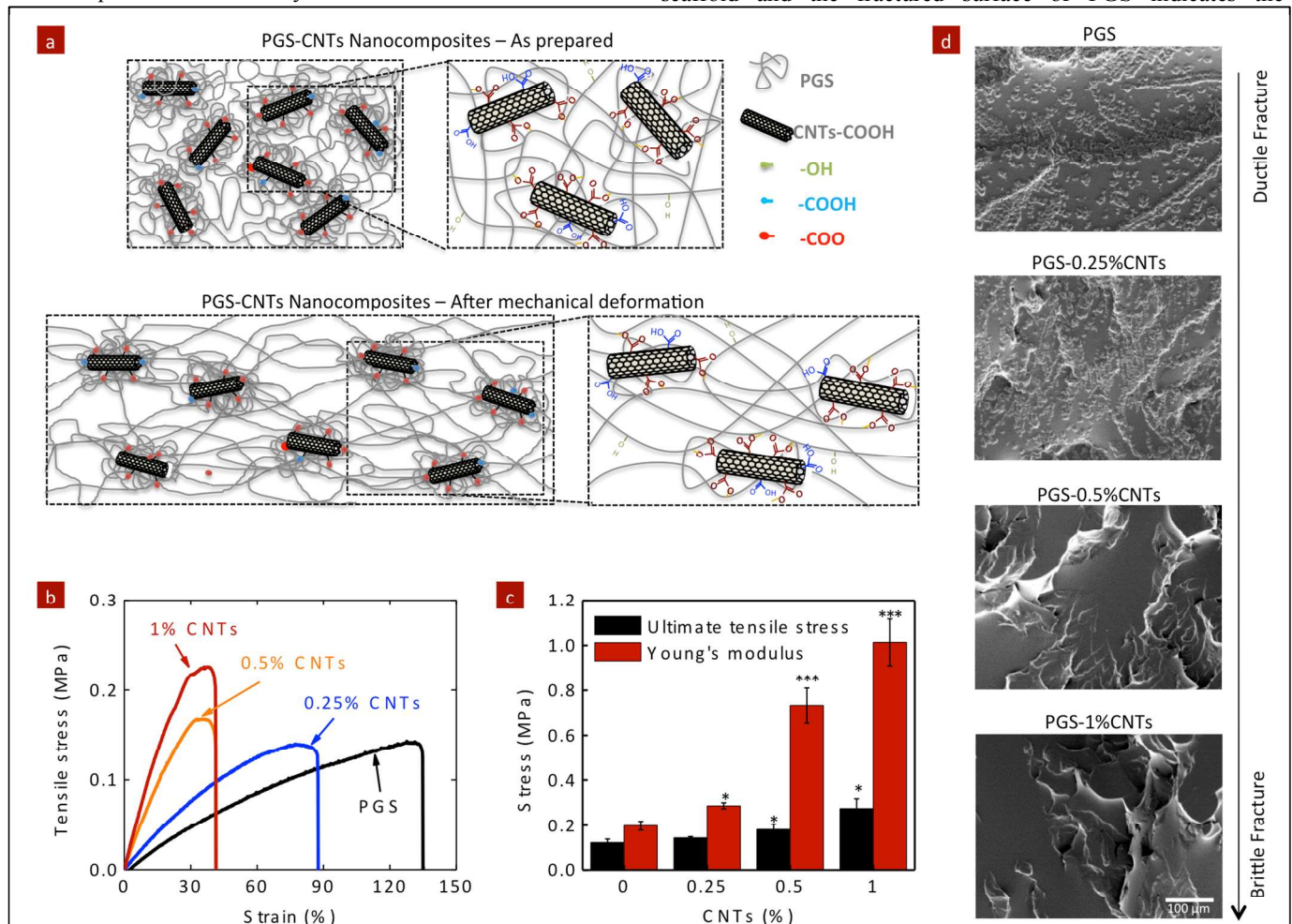

Figure 4: Effect of CNTs on the tensile properties of PGS-CNTs nanocomposites. (a) CNTs act as a physical and covalent crosslinker, and result in increase in mechanical stiffness of PGS network by increasing the crosslinking density. (b) The addition of CNTs (0.25, 0.5 and 1%) to PGS results in significant increase in the Young's modulus and ultimate tensile stress of the nanocomposite network. (c) By addition of only 1% CNT, almost a five-fold increment in Young's modulus was observed, whereas the ultimate tensile stress increased more than two folds. (d) SEM images of fractured surfaces of PGS-CNTs nanocomposites after tensile testing show the fracture mechanism dominating the nanocomposite network. PGS is an elastomeric polymer and show ductile fracture. The addition of CNTs reinforces the PGS network due to covalent crosslinking and results in brittle fracture. (One-way ANOVA with Tukey post-hoc analysis, *p<0.05, ***p<0.001).

formation of stress concentration that ultimately leads to failure. As the amount of CNTs increases, the fracture mode changes from a ductile fracture to a brittle fracture. In nanocomposites containing 0.5 and 1%, CNTs showed minimum surface deformation and the fracture surface displayed a relatively smooth surface morphology typically observed in a brittle fracture.

Elastomeric properties of PGS-CNTs nanocomposites

The elastomeric properties of PGS-CNTs nanocomposites were investigated using unconfined cyclic compression (Figure 5a). The compressive modulus of pure PGS was determined to be 0.66 ± 0.07 MPa. The addition of 0.25%, 0.50%, and 1% CNTs significantly increases (*$p<0.05$) compressive modulus of the nanocomposites to 1.73 ± 0.09, 3.34 ± 0.06, and 4.06 ± 0.11 MPa, respectively. The addition of 1% CNTs to PGS results in more than a six-fold increase in the compressive modulus, which is far superior to the mechanical properties previously

may be attributed to the strong covalent interactions between PGS and CNTs that restricts polymer chain movement during mechanical deformation.

The effect of CNTs on energy absorbed by the network during the cyclic compression was also evaluated (Figure 5b & c). The nanocomposite scaffolds were subjected to five loading and unloading curves until 20% strain. The energy absorbed by the network during deformation and the recovery of network after the deformation was determined. Pure PGS showed energy absorbed of 0.99 ± 0.36 kJ/m^3 (recovery $\sim 95\pm1.4$%) during the first cycle and subsequent cycles (2-5 cycles) showed energy absorbed of 0.5 ± 0.03 kJ/m^3 (recovery $\sim 99.2\pm0.3$%). The addition of CNTs significantly enhances (*$p<0.05$) the amount of energy absorbed without compromising elastic recovery of the network. For example, nanocomposites containing 1% CNTs showed energy absorbed of 6.66 ± 0.64 kJ/m^3 (recovery $\sim 94.9\pm1.2$%) for the first cycle and the subsequent cycles (2-5 cycles) showed energy absorbed
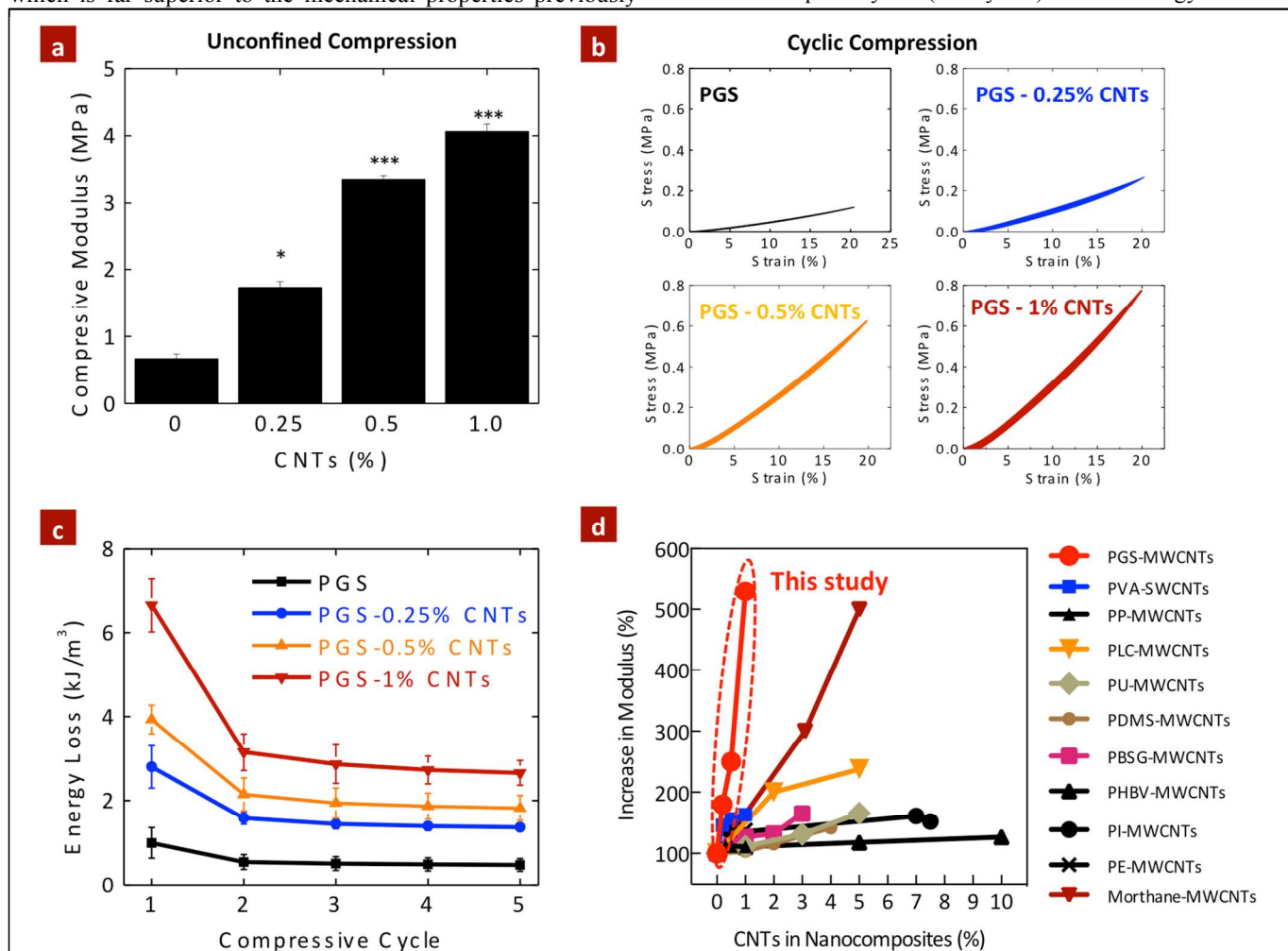
Figure 5: Effect of CNTs on compression properties of PGS-CNTs nanocomposites. (a) The addition of CNTs to PGS network result in significantly increase in compressive modulus of the nancomposites. (b) Cyclic compression of PGS and PGS-CNTs indicates elastomeric properties of PGS network is preserved. (c) The energy absorbed by the network during cyclic deformation of network indicates maximum loss in energy during the first cycle. In subsequent cycle the energy loss was constant for the network. (d) The increase in mechanical stiffness due to addition of CNTs to different polymeric matrix is summarized (PVA[50], PLGA[51], PP[52], PLC[53], PU[54], PDMS[55], PBSG[56], PHBV[57], PI[58], PE[59], Morthane[60]). These data has been re-plotted from published reports. Most of the earlier studies have reported a moderate 20-300% increase in modulus due to the addition of 1 to 10% of CNTs. Current study (PGS-CNTs) showed more than 500% increase in modulus of polymeric networks by the addition of 1% CNTs, which is not reported previously. (One-way ANOVA with Tukey post-hoc analysis, *$p<0.05$, ***$p<0.001$).

reported for CNT-based nanocomposites.[43, 50-61]. This increase

of 2.85 ± 0.22 kJ/m^3 (recovery $\sim 98.9\pm0.3$%). Thus the

incorporation of CNTs to PGS network results in significant increase in mechanical stiffness without compromising elasticity of the nanocomposite networks. This is mainly attributed to the esterification of carboxyl groups of CNTs with the PGS backbone that results in improved load transfer efficiency within the crosslinked network.

Overall, the mechanical stiffness due to addition of CNTs in both compression and tension has been shown to increase by five-fold. This is an improvement compared to earlier studies[43] that have reported a moderate 20-300% increase in modulus due to the addition of 1 to 10% of CNTs as summarized in Figure 5d. For example, So et al. showed a 30% increase in modulus due to the addition of 5% of COOH-modified-CNTs to polyimide (PI).[58] Cha et al., showed a ~260% increase in modulus due to the addition of 10% CNTs to copper nanocomposites.[61] In a similar study, Koerner et al. reinforced thermoplastic elastomer (Morthane) with 1-5% CNTs and observed a 200-500% increase in modulus.[60] They attributed the significant increase in mechanical properties to the formation of a percolation network.[60] In another study, Lahiri et al. showed that the addition of 2 and 5% CNTs to poly(L-lactide-co-caprolactone) (PLC) results in two-fold and 2.4-fold increases in modulus, respectively.[53] Jell et al. developed CNTs-reinforced polyurethane (PU) scaffolds using a thermally induced phase separation method and was able to enhance the compressive modulus by two-folds by adding 5% CNTs.[54] In a similar study, Armentano et al. synthesized poly(DL-lactide-co-glycolide) (PLGA 50:50) nanocomposite by incorporating pristine and carboxyl functionalized single-walled CNTs.[51] The elastic modulus of PLGA improved more than 300% due to the addition of 1% CNT.[51] The addition of 1% multiwalled CNTs to polyethylene (PE) films also resulted in moderate increase in tensile strength (125%).[59] Hou et al., also showed relatively moderate increase (~132%) in mechanical stiffness of polyvinyl alcohol (PVA) due to addition of single-walled and multiwalled CNTs.[50] Other polymers such as poly(dimethylsiloxane) (PDMS)[55], polypropylene (PP)[52], poly(butylene succinate-co-ethylene glycol) (PBSG)[56], poly(3-hydroxybutyrate-co-3-hydroxyvalerate) (PHBV)[57] also showed moderate increase in mechanical properties as shown in Figure 5d. The results reported here (PGS-CNTs) are quite unique as more than 500% modulus of polymeric networks can be enhanced by just the addition of 1% CNTs. Moreover, the synthesis technique to obtain PGS-CNTs nanocomposites is relatively simple and does not require extensive post-processing.

In vitro stability of PGS-CNTs nanocomposites

For biomedical and biotechnological applications, it is important to investigate the in vitro stability of nanocomposite biomaterials. The surface characteristic and in vitro degradation of PGS-CNTs nanocomposites were determined under a physiological environment. It is expected that the addition of CNTs to PGS should increase the in vitro stability of nanocomposites due to the increase in the crosslinking density due to addition of CNTs.

The surface characteristic of PGS and PGS-CNTs nanocomposites was determined using optical tensiometry (goniometry). The esterification of carboxyl groups of CNTs with hydroxyl groups of PGS, reduces the hydrophilic nature of the nanocomposites. The contact angle of a sessile water drop on the nanocomposite surface was used to determine the hydrophilicity of the material (Figure 6a & b). The contact

angle of the PGS surface was observed to be 69.78±1.39°, similar to the previously reported literature.[40] Incorporation of CNTs to the PGS network significantly enhances the contact angle of water. The addition of 0.25%, 0.5%, and 1% CNTs to PGS increases the contact angle of water to 71.01±1.26°, 78.54±1.65°, and 79.63±1.10°. This result was further supported by evaluating hydration degree of nanocomposites (Figure 6c). The addition of CNTs significantly reduces water uptake ability of the nanocomposites. It is expected that this may also retard degradation of polyester backbone and also alter the interaction of nanocomposites with biological entities such as proteins and cells.

PGS degrades via surface erosion mechanism and display linear degradation behavior under in vitro and in vivo conditions.[36, 45] A linear degradation behavior is preferable for tissue engineered scaffolds to follow with the ECM biosynthesis rate. The degradation properties of PGS and PGS-CNTs nanocomposites were determined in physiological conditions (PBS, 37°C). From the contact angle measurements results, it was observed that the addition of CNTs decreases hydrophilicity of the nanocomposites network; thus, it was expected that the addition of CNTs should result in a decrease in the degradation rate of the nanocomposites.

Under in vivo conditions, PGS degraded relatively fast compared to in vitro conditions. The fast in vivo degradation of PGS is attributed to the presence of esterases in the surrounding microenvironment that accelerates the degradation process. In order to closely mimic the in vivo degradation, PGS and PGS-CNTs nanocomposites were subjected to 0.01M NaOH that also accelerates the rate of degradation through alkaline-catalyzed conditions. The mass loss of PGS and PGS-CNTs nanocomposites in 0.01M NaOH was monitored over 30 days (Figure 6d). All samples follow a linear degradation without compromising the structural integrity. After 30 days, the mass loss for PGS was 49.4±2.8% (degradation rate ~11.5%/week), addition of 0.25%, 0.50%, and 1% of CNTs results in mass loss (degradation rate) of 44.8±1.7% (~10.5%/week), 25.8±2.2% (~6%/week), and 21.3±0.8% (~5%/week), respectively. The mass loss data indicates that with an increase in CNTs concentration, the rate of degradation decreases.

Compared to earlier studies with polyester-carboxyl functionalized CNT nanocomposites, the covalently crosslinked PGS-CNTs nanocomposites reported here showed opposite trends in degradation behavior. For example, Armentano et al. analyzed the in vitro degradation behavior of PLGA-CNTs nanocomposites where it was observed that the presence of carboxyl functionalized CNTs induced faster degradation of nanocomposites.[62] Zhao et al. also observed similar trends in the PLLA-CNT nanocomposites system.[63] In both of these studies, the functionalized CNTs were physically entrapped within the polyester structures and no covalent interactions of CNTs with the polymer backbone were observed.[62, 63] Moreover, due to the hydrophilic nature of carboxyl groups present on functionalized CNTs also enhanced the hydration ability within polyester nanocomposites and resulted in the accelerated degradation. Thus, the degradation data in PGS-CNTs nanocomposites also indirectly demonstrated the esterification of carboxyl functionalized CNTs within PGS network.

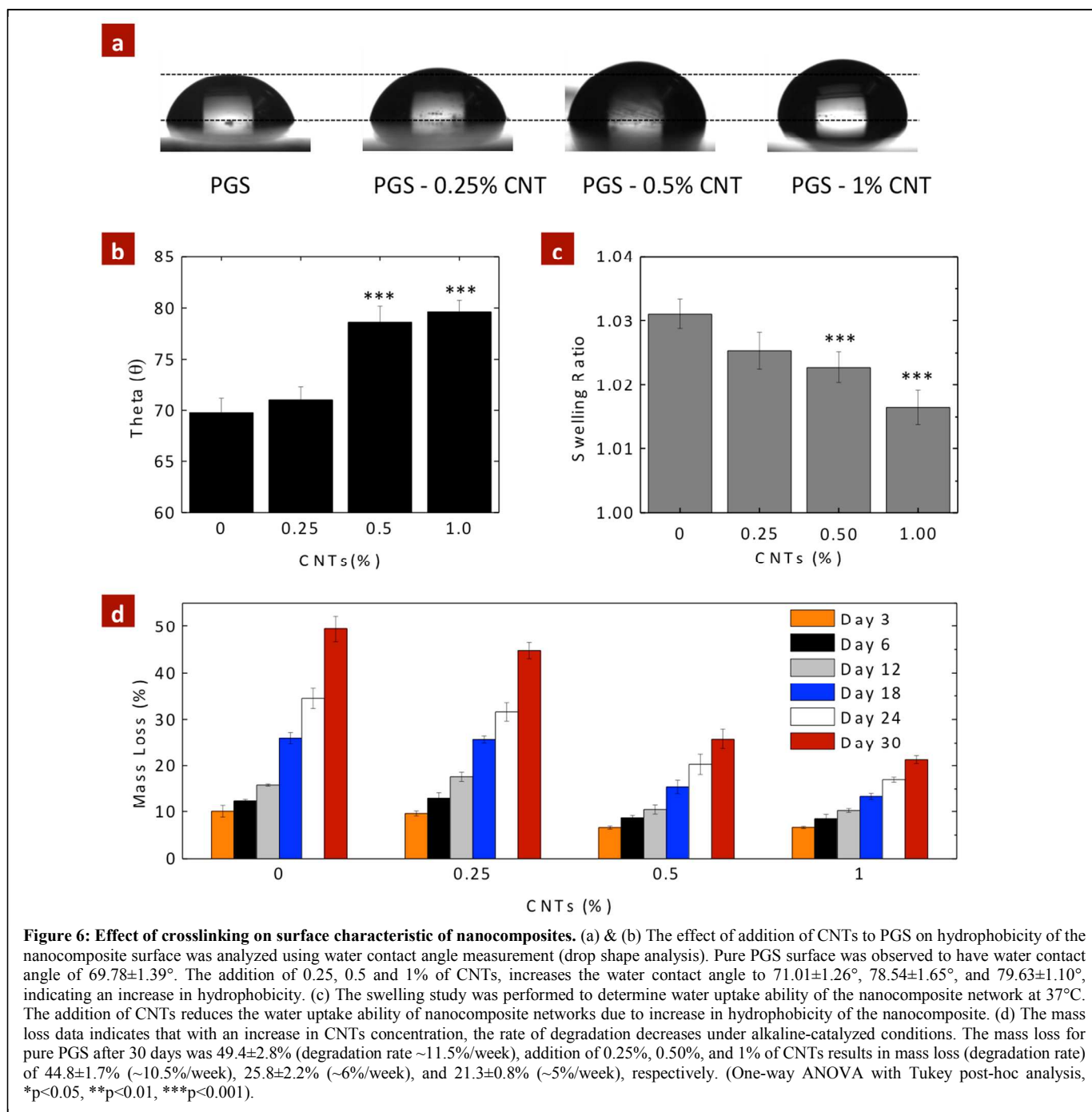### hMSCs adhesion, proliferation, and differentiation on PGS-CNTs nanocomposites

Figure 6: Effect of crosslinking on surface characteristic of nanocomposites. (a) & (b) The effect of addition of CNTs to PGS on hydrophobicity of the nanocomposite surface was analyzed using water contact angle measurement (drop shape analysis). Pure PGS surface was observed to have water contact angle of 69.78±1.39°. The addition of 0.25, 0.5 and 1% of CNTs, increases the water contact angle to 71.01±1.26°, 78.54±1.65°, and 79.63±1.10°, indicating an increase in hydrophobicity. (c) The swelling study was performed to determine water uptake ability of the nanocomposite network at 37°C. The addition of CNTs reduces the water uptake ability of nanocomposite networks due to increase in hydrophobicity of the nanocomposite. (d) The mass loss data indicates that with an increase in CNTs concentration, the rate of degradation decreases under alkaline-catalyzed conditions. The mass loss for pure PGS after 30 days was 49.4±2.8% (degradation rate ~11.5%/week), addition of 0.25%, 0.50%, and 1% of CNTs results in mass loss (degradation rate) of 44.8±1.7% (~10.5%/week), 25.8±2.2% (~6%/week), and 21.3±0.8% (~5%/week), respectively. (One-way ANOVA with Tukey post-hoc analysis, *$p<0.05$, **$p<0.01$, ***$p<0.001$).

To evaluate the feasibility of the PGS-CNTs nanocomposite network for tissue engineering applications, cell-matrix interactions were evaluated using hMSCs. PGS and PGS-CNT nanocomposite were seeded with hMSCs, to determine the effect of CNTs on metabolic activity and ALP production. The metabolic activity of adhered hMSCs was determined using Alamar Blue assay for 10 days (Figure 7a). Compared to the TCPS control, the metabolic activity of seeded hMSCs was almost half on PGS and PGS-CNTs surfaces. However, no significant difference in the metabolic activity of seeded hMSCs was observed due to the addition of CNTs. The *in vitro* study was carried out for 10 days and all scaffolds were intact during this time frame. Under *in vivo* conditions, PGS might

degrade and entrapped CNTs might come out. It is expected that these CNTs might results in mild inflammation and fibrosis. However, additional *in vivo* studies are needed to determine the long-term efficacy of PGS-CNTs nanocomposites.

Having established the ability to support hMSCs proliferation, we investigated the potential of PGS-CNTs nanocomposite for orthopaedic tissue engineering by monitoring the osteogenic differentiation of hMSCs. We monitored ALP activity on 7, 14 and 21 day, and calcium production on 14 and 21 day. ALP is an early marker and hallmark for osteogenesis. The addition of CNTs, resulted in significant (*$p<0.05$) upregulation of ALP production on PGS-
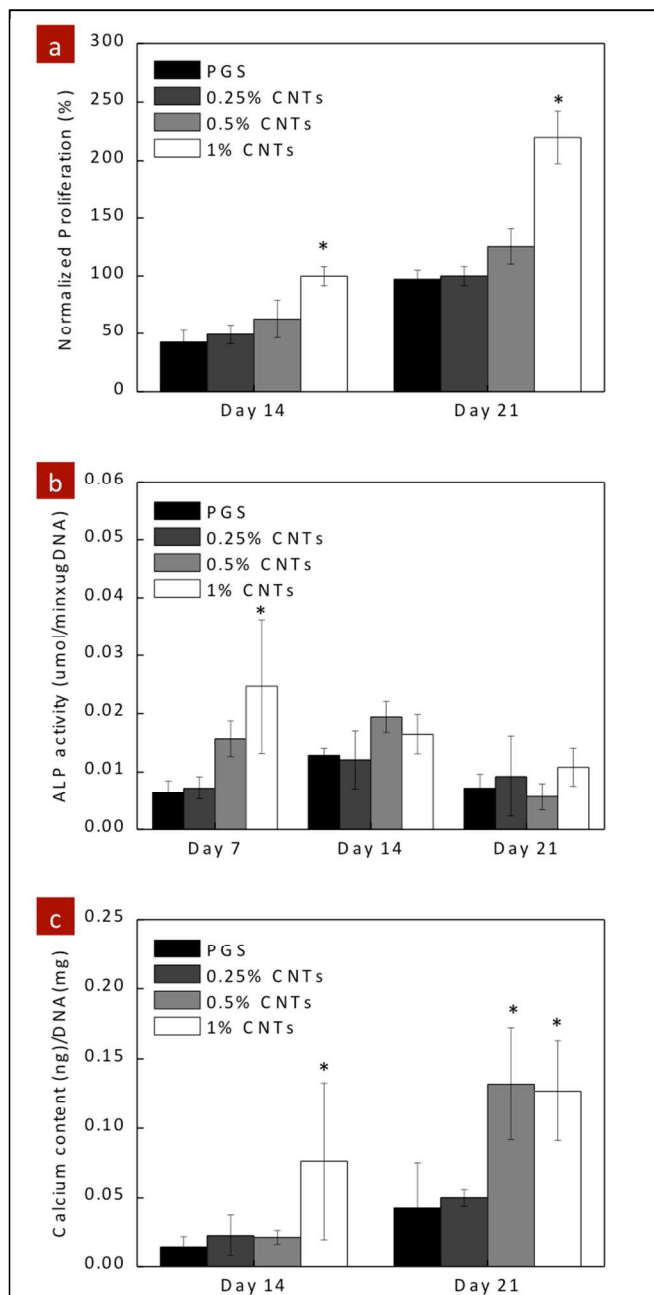
Figure 7: *In vitro* **evaluation of PGS-CNTs nanocomposite using hMSCs.** (a) PGS and PGS-CNTs nanocomposite support proliferation of hMSCs. Tissue culture polystyrene (TCPS) surface was used as positive control. (b) ALP activity of hMSCs seeded on PGS and PGS-CNTs was monitored on days 7, 14 and 21. The peak ALP activity (day 7) on PGS-1%CNTs nanocomposite was significantly higher compared to PGS. No significant effect was observed on days 14 and 21. (c) The amount of calcium deposited by hMSCs was significantly higher on PGS-1%CNTs compared to PGS. (One-way ANOVA with Tukey post-hoc analysis, *p<0.05).

significant difference was observed. But on day 21, nanocomposites containing 1% and 0.5% CNTs show significantly (*p<0.05) higher amount of calcium compared to PGS scaffolds (Figure 7c). The increase in ALP expression and calcium production might be attributed to the increase in surface hydrophobicity, change in surface topography and increase in stiffness due to the addition of the CNTs to the PGS networks.

Conclusions

We have successfully designed and developed stiff, elastomeric nanocomposites from PGS and CNTs. To our knowledge, this is the first attempt to physically entrap and covalently conjugate the CNTs within PGS structure. Imaging techniques revealed a uniform distribution of CNTs within PGS network. The addition of 1% CNTs to PGS, result in five-fold increase in tensile modulus and six-fold increase in compressive modulus. The reported increase in mechanical properties is much superior compared to previously published literature for CNT-based nanocomposites. Despite significant increase in mechanical stiffness, the elasticity of the network was not compromised and all the nanocomposites showed more than 94% recovery. The strong covalent interactions between PGS and CNTs restrict polymer chains movement during mechanical deformation and result in novel property combinations that are not observed in conventional nanocomposites. The addition of CNTs to PGS increases the surface hydrophobicity of nanocomposite and thus reduces the degradation rate up to 40% compared to PGS. Additionally, *in vitro* studies using hMSCs indicated that the addition of CNTs to PGS support the differentiation potential of the seeded hMSCs as indicated by increase in ALP activity and production of calcium. Overall, the unique property combinations of ultra-stiff, elastomeric CNT-PGS nanocomposites make them potentially suitable for biomedical applications such as scaffolding in musculoskeletal tissue engineering.

1%CNTs compared to pure PGS (Figure 7b). This indicates that stiffness of the nanocomposite may play a significant role in osteogenesis. As expected on days 14 and 21, no significant difference in the ALP activity was observed. Similar trend was observed in calcium production on days 14 and 21. The nanocomposite containing 1% CNTs show slightly higher amount of calcium on day 14 compared to PGS, although no

Notes

[a]David H. Koch Institute for Integrative Cancer Research, Massachusetts Institute of Technology, Cambridge, MA 02139 (USA).

[b]Wyss Institute for Biologically Inspired Engineering, Harvard University, Boston, MA 02115 (USA).

[c]Biomaterials Innovation Research Center, Division of Biomedical Engineering, Department of Medicine, Brigham and Women's Hospital, Harvard Medical School, Cambridge, MA 02139 (USA).

[d]Harvard-MIT Division of Health Sciences and Technology, Massachusetts Institute of Technology, Cambridge, MA 02139 (USA).

[e]Department of Electrical and Computer Engineering (Biomedical Engineering Option), King Abdulaziz University, Jeddah 21589, Saudi Arabia

[f]Department of Maxillofacial Biomedical Engineering and Institute of Oral Biology, School of Dentistry, Kyung Hee University, Seoul 130-701, Republic of Korea.

[g]Department of Physics, King Abdulaziz University, Jeddah 21569, Saudi Arabia.

[x]Currently at: Department of Biomedical Engineering and Department of Materials Science and Engineering, Texas A&M University, College Station, TX 77843 (USA)

[α]Currently at: Interdisciplinary Nanoscience Center (iNANO), Aarhus University, Aarhus (8000), Denmark

[‡]Dr. A.K.Gaharwar and Dr. A. Patel contributed equally

E-mail: alik@rics.bwh.harvard.edu (Prof. Ali Khademhosseini); gaharwar@tamu.edu (Prof. Akhilesh K. Gaharwar)
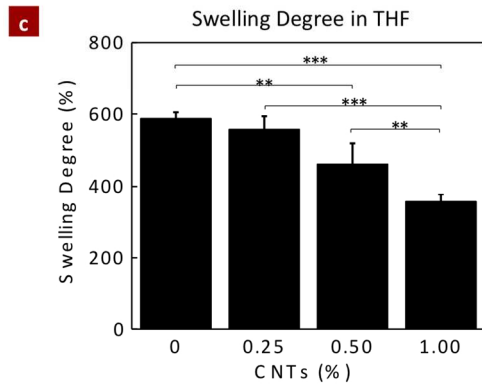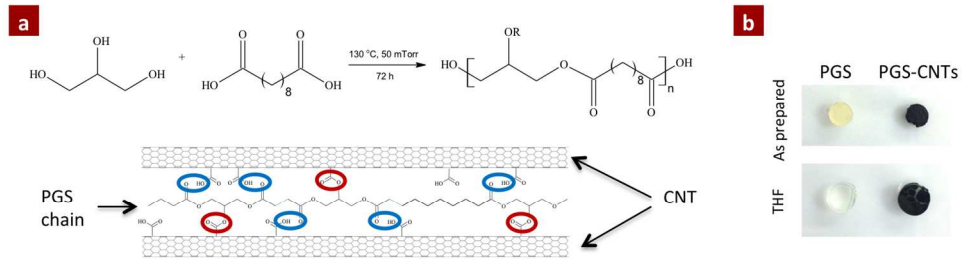
References

1. A. Oberlin, M. Endo and T. Koyama, *Journal of Crystal Growth*, 1976, 32, 335-349.
2. S. Iijima, *Nature*, 1991, 354, 56-58.
3. R. H. Baughman, A. A. Zakhidov and W. A. de Heer, *Science*, 2002, 297, 787-792.
4. A. Fennimore, T. Yuzvinsky, W.-Q. Han, M. Fuhrer, J. Cumings and A. Zettl, *Nature*, 2003, 424, 408-410.
5. R. H. Baughman, C. Cui, A. A. Zakhidov, Z. Iqbal, J. N. Barisci, G. M. Spinks, G. G. Wallace, A. Mazzoldi, D. De Rossi and A. G. Rinzler, *Science*, 1999, 284, 1340-1344.
6. K. Mylvaganam and L. Zhang, *Nanotechnology*, 2007, 18, 475701.
7. E. Fortunati, F. D'Angelo, S. Martino, A. Orlacchio, J. M. Kenny and I. Armentano, *Carbon*, 2011, 49, 2370-2379.
8. T. Kashiwagi, F. Du, J. F. Douglas, K. I. Winey, R. H. Harris, Jr. and J. R. Shields, *Nature Materials*, 2005, 4, 928-933.
9. A. C. Dillon, K. Jones, T. Bekkedahl, C. Kiang, D. Bethune and M. Heben, *Nature*, 1997, 386, 377-379.
10. B. S. Harrison and A. Atala, *Biomaterials*, 2007, 28, 344-353.
11. L. P. Zanello, B. Zhao, H. Hu and R. C. Haddon, *Nano letters*, 2006, 6, 562-567.
12. L. Lacerda, S. Raffa, M. Prato, A. Bianco and K. Kostarelos, *Nano Today*, 2007, 2, 38-43.
13. A. Bianco, K. Kostarelos and M. Prato, *Current opinion in chemical biology*, 2005, 9, 674.
14. K. Besteman, J.-O. Lee, F. G. Wiertz, H. A. Heering and C. Dekker, *Nano letters*, 2003, 3, 727-730.
15. J. Wang, *Electroanalysis*, 2005, 17, 7-14.
16. A. K. Hüttel, G. A. Steele, B. Witkamp, M. Poot, L. P. Kouwenhoven and H. S. J. van der Zant, *Nano letters*, 2009, 9, 2547-2552.
17. S. Sarojini, S. Rajasekar and K. Koumaravelou, *International Journal of Pharma and Bio Sciences*, 2010, 1, 644-649.
18. P. A. Tran, L. Zhang and T. J. Webster, *Advanced Drug Delivery Reviews*, 2009, 61, 1097-1114.
19. X. Chen, A. Kis, A. Zettl and C. R. Bertozzi, *Proceedings of the National Academy of Sciences*, 2007, 104, 8218-8222.
20. A. K. Gaharwar, N. A. Peppas and A. Khademhosseini, *Biotechnology and Bioengineering*, 2014, DOI: 10.1002/bit.25160.
21. A. K. Gaharwar, C. Rivera, C.-J. Wu, B. K. Chan and G. Schmidt, *Materials Science and Engineering: C*, 2013, 33, 1800-1807.
22. S. Goenka, V. Sant and S. Sant, *Journal of Controlled Release*, 2013.
23. M. Shim, N. W. Shi Kam, R. J. Chen, Y. Li and H. Dai, *Nano letters*, 2002, 2, 285-288.
24. P.-C. Ma, N. A. Siddiqui, G. Marom and J.-K. Kim, *Composites Part A: Applied Science and Manufacturing*, 2010, 41, 1345-1367.
25. X.-L. Xie, Y.-W. Mai and X.-P. Zhou, *Materials Science and Engineering: R: Reports*, 2005, 49, 89-112.
26. A. Hirsch and O. Vostrowsky, in *Functional molecular nanostructures*, Springer, 2005, pp. 193-237.
27. H. Peng, L. B. Alemany, J. L. Margrave and V. N. Khabashesku, *Journal of the American Chemical Society*, 2003, 125, 15174-15182.
28. L. Zhang, V. U. Kiny, H. Peng, J. Zhu, R. F. Lobo, J. L. Margrave and V. N. Khabashesku, *Chemistry of materials*, 2004, 16, 2055-2061.
29. Y. Wang, Z. Iqbal and S. V. Malhotra, *Chemical physics letters*, 2005, 402, 96-101.
30. H. Wang, *Current Opinion in Colloid & Interface Science*, 2009, 14, 364-371.
31. S. S. Karajanagi, H. Yang, P. Asuri, E. Sellitto, J. S. Dordick and R. S. Kane, *Langmuir*, 2006, 22, 1392-1395.
32. M. Zheng, A. Jagota, E. D. Semke, B. A. Diner, R. S. McLean, S. R. Lustig, R. E. Richardson and N. G. Tassi, *Nature materials*, 2003, 2, 338-342.
33. J. N. Coleman, U. Khan and Y. K. Gun'ko, *Advanced Materials*, 2006, 18, 689-706.
34. T. Liu and S. Guo, *Properties of Polyurethane/Carbon Nanotube Nanocomposites*, Scrivener Publishing, 2010.
35. K. Hayashida and H. Tanaka, *Advanced Functional Materials*, 2012, 22, 2338-2344.
36. Y. Wang, Y. M. Kim and R. Langer, *Journal of Biomedical Materials Research Part A*, 2003, 66A, 192-197.
37. Y. D. Wang, G. A. Ameer, B. J. Sheppard and R. Langer, *Nat. Biotechnol.*, 2002, 20, 602-606.
38. A. R. Webb, J. Yang and G. A. Ameer, *Expert Opinion on Biological Therapy*, 2004, 4, 801-812.
39. R. Rai, M. Tallawi, A. Grigore and A. R. Boccaccini, *Progress in Polymer Science*, 2012, 37, 1051-1078.
40. A. Patel, A. K. Gaharwar, G. Iviglia, H. Zhang, S. Mukundan, S. M. Mihaila, D. Demarchi and A. Khademhosseini, *Biomaterials*, 2013, 34, 3970-3983.
41. J. Y. Kim, *Poly(butylene terephthalate) Nanocomposites Containing Carbon Nanotube*, Advances in Nanocomposites - Synthesis, Characterization and Industrial Applications.
42. J. Y. Kim, S. I. Han and S. Hong, *Polymer*, 2008, 49, 3335-3345.
43. N. G. Sahoo, S. Rana, J. W. Cho, L. Li and S. H. Chan, *Progress in Polymer Science*, 2010, 35, 837-867.
44. M. S. Dresselhaus, A. Jorio, M. Hofmann, G. Dresselhaus and R. Saito, *Nano letters*, 2010, 10, 751-758.
45. I. Pomerantseva, N. Krebs, A. Hart, C. M. Neville, A. Y. Huang and C. A. Sundback, *Journal of Biomedical Materials Research Part A*, 2009, 91, 1038-1047.
46. S. Huang, M. Wang, T. Liu, W.-D. Zhang, W. C. Tjiu, C. He and X. Lu, *Polymer Engineering & Science*, 2009, 49, 1063-1068.
47. J. Y. Kim, S. Han, D. K. Kim and S. H. Kim, *Composites: Part A*, 2009, 40, 45-53.
48. W. Cai and C. Liu, *Mater Lett*, 2008, 62, 2171-2173.
49. S. L. Liang, W. D. Cook, G. A. Thouas and Q. Z. Chen, *Biomaterials*, 2010, 31, 8516-8529.
50. Y. Hou, J. Tang, H. Zhang, C. Qian, Y. Feng and J. Liu, *ACS nano*, 2009, 3, 1057-1062.
51. I. Armentano, M. Dottori, D. Puglia and J. M. Kenny, *Journal of Materials Science: Materials in Medicine*, 2007, 19, 2377-2387.
52. A. A. Kovalchuk, V. G. Shevchenko, A. N. Shchegolikhin, P. M. Nedorezova, A. N. Klyamkina and A. M. Aladyshev, *Journal of Materials Science*, 2008, 43, 7132-7140.
53. D. Lahiri, F. Rouzaud, T. Richard, A. K. Keshri, S. R. Bakshi, L. Kos and A. Agarwal, *Acta biomaterialia*, 2010, 6, 3524-3533.
54. G. Jell, R. Verdejo, L. Safinia, M. S. P. Shaffer, M. M. Stevens and A. Bismarck, *Journal of Materials Chemistry*, 2008, 18, 1865-1872.
55. C.-L. Wu, H.-C. Lin, J.-S. Hsu, M.-C. Yip and W. Fang, *Thin Solid Films*, 2009, 517, 4895-4901.
56. L. Tan, Y. Chen, W. Zhou and S. Ye, *Polymer Engineering & Science*, 2012, 52, 2506-2517.
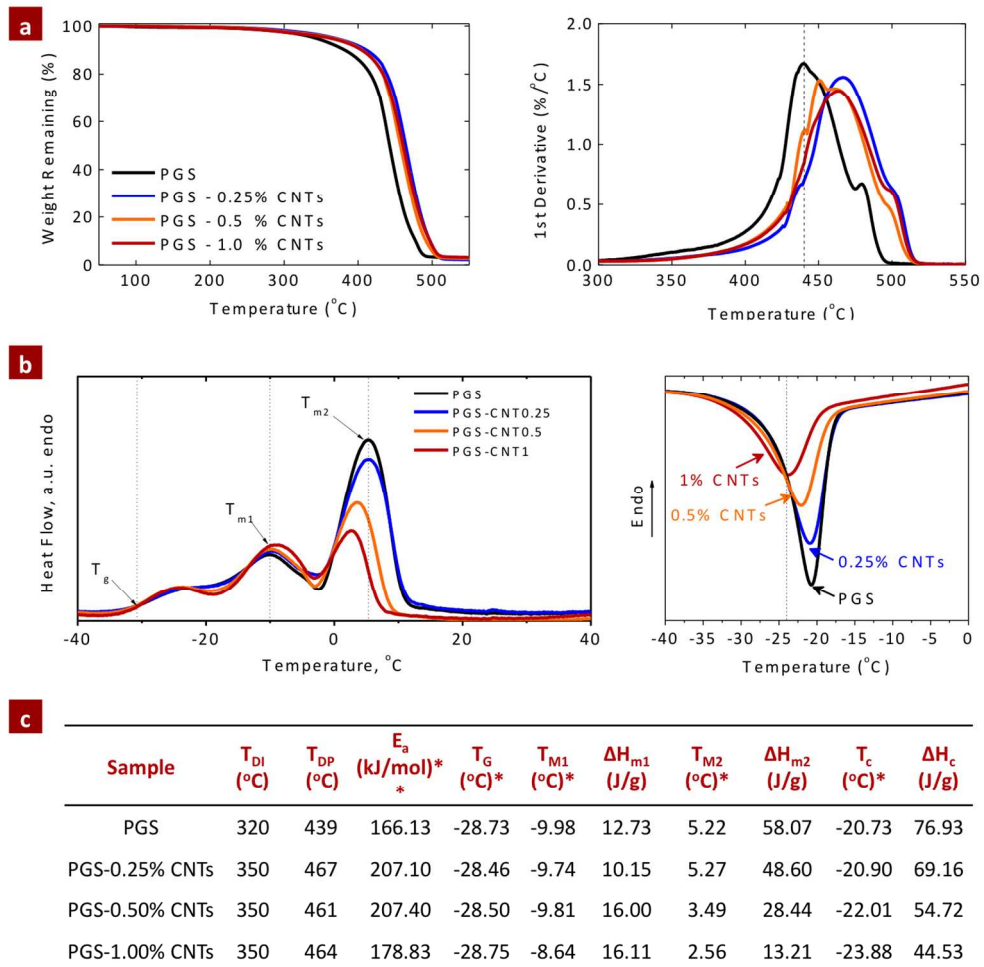
57.   S. Vidhate, L. Innocentini Mei and N. A. D'Souza, *Polymer Engineering & Science*, 2012, 52, 1367-1374.
58.   H. H. So, J. W. Cho and N. G. Sahoo, *European Polymer Journal*, 2007, 43, 3750-3756.
59.   S. Ruan, P. Gao, X. Yang and T. Yu, *Polymer*, 2003, 44, 5643-5654.
60.   H. Koerner, G. Price, N. A. Pearce, M. Alexander and R. A. Vaia, *Nature materials*, 2004, 3, 115-120.
61.   S. I. Cha, K. T. Kim, S. N. Arshad, C. B. Mo and S. H. Hong, *Advanced Materials*, 2005, 17, 1377-1381.
62.   I. Armentano, M. Dottori, D. Puglia and J. M. Kenny, *J Mater Sci Mater Med*, 2008, 19, 2377-2387.
63.   Y. Zhao, Z. Qiu and W. Yang, *Composites Science and Technology*, 2009, 69, 627-632.
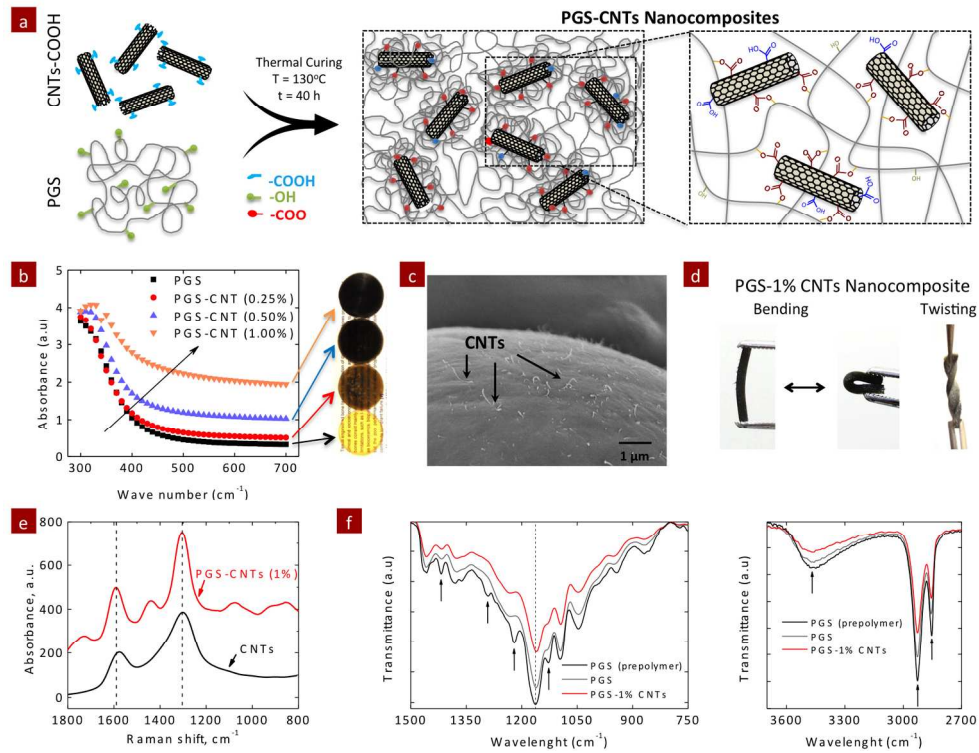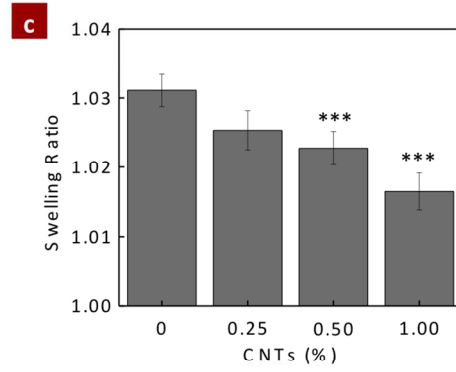
705x529mm (72 x 72 DPI)

583x425mm (72 x 72 DPI)

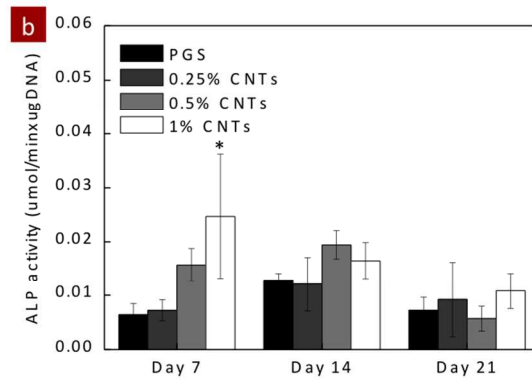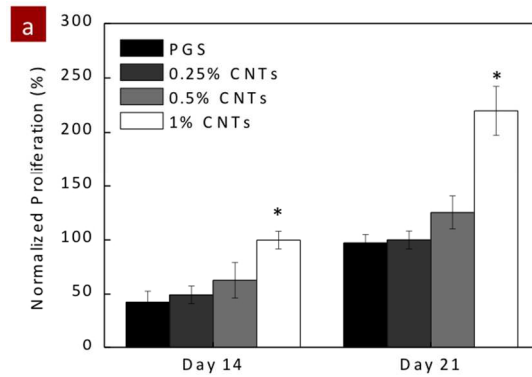| Sample	T_{DI} (°C)	T_{DP} (°C)	E_a (kJ/mol)**	T_G (°C)*	T_{M1} (°C)*	ΔH_{m1} (J/g)	T_{M2} (°C)*	ΔH_{m2} (J/g)	T_c (°C)*	ΔH_c (J/g)
PGS	320	439	166.13	-28.73	-9.98	12.73	5.22	58.07	-20.73	76.93
PGS-0.25% CNTs	350	467	207.10	-28.46	-9.74	10.15	5.27	48.60	-20.90	69.16
PGS-0.50% CNTs	350	461	207.40	-28.50	-9.81	16.00	3.49	28.44	-22.01	54.72
PGS-1.00% CNTs	350	464	178.83	-28.75	-8.64	16.11	2.56	13.21	-23.88	44.53
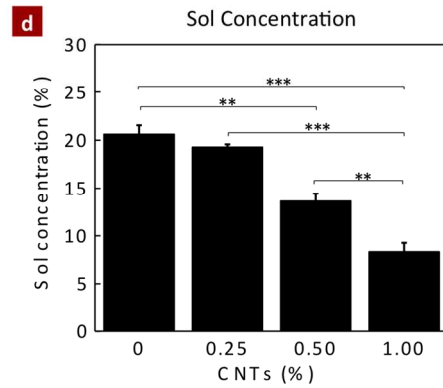
530x523mm (72 x 72 DPI)
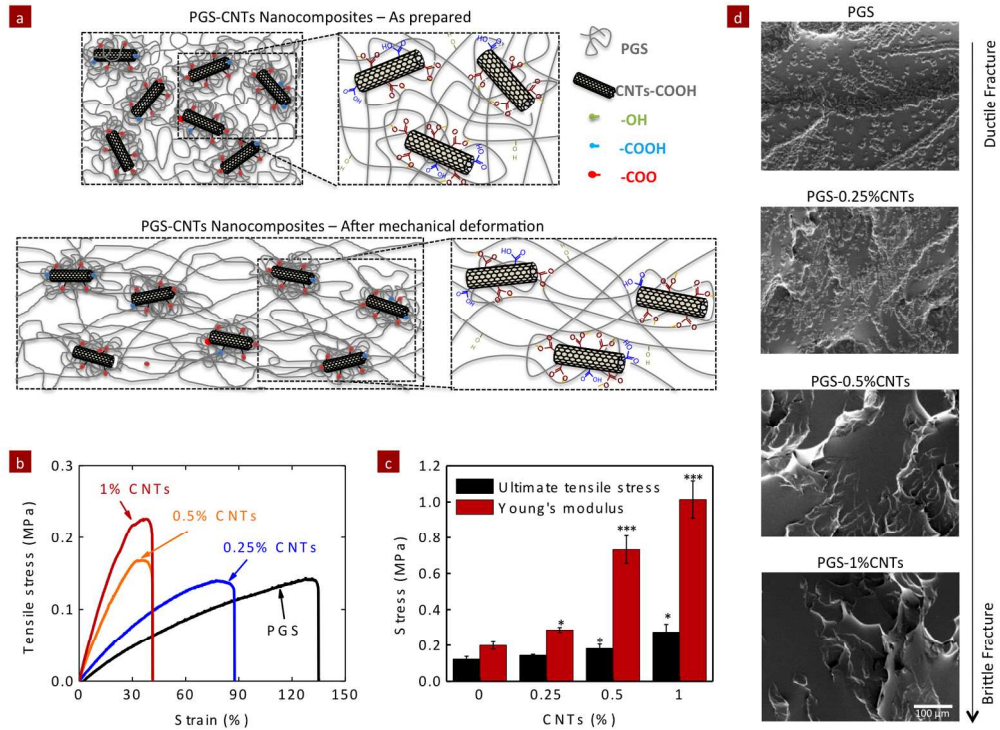
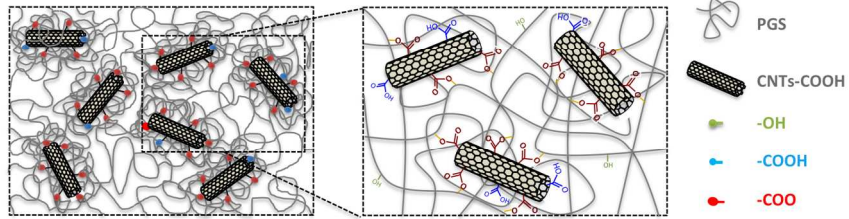705x529mm (72 x 72 DPI)
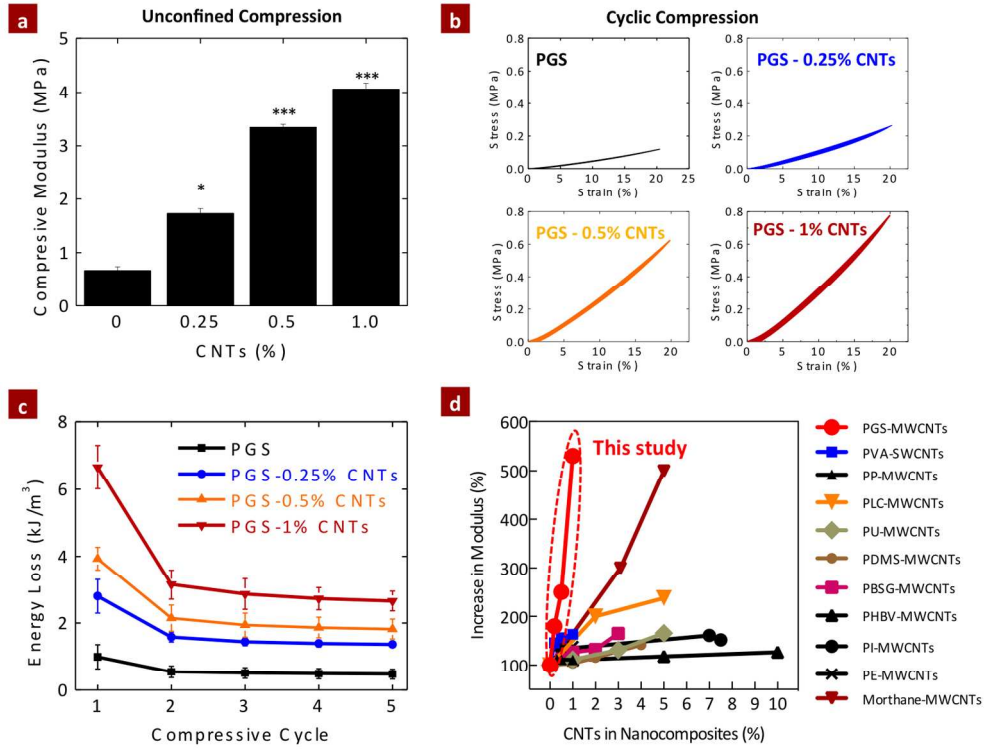
612x470mm (72 x 72 DPI)
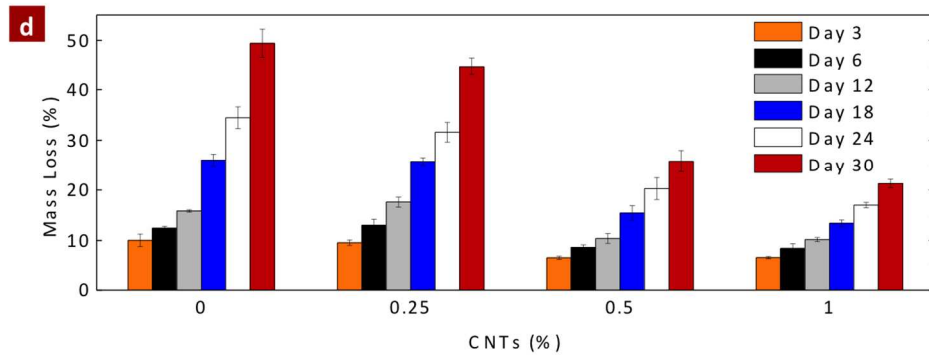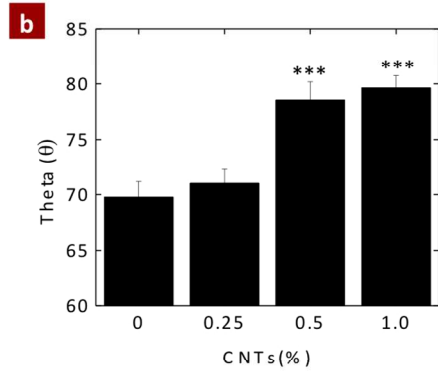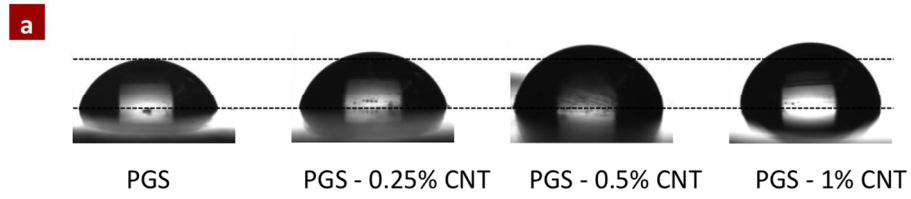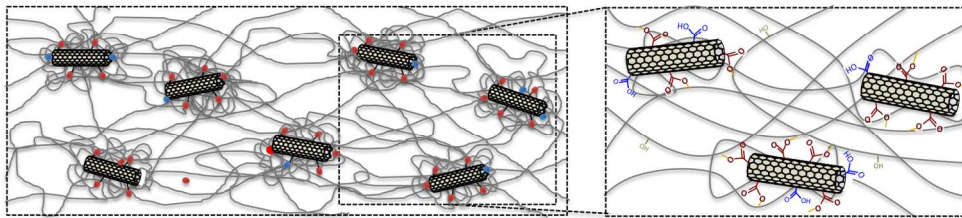
495x486mm (72 x 72 DPI)
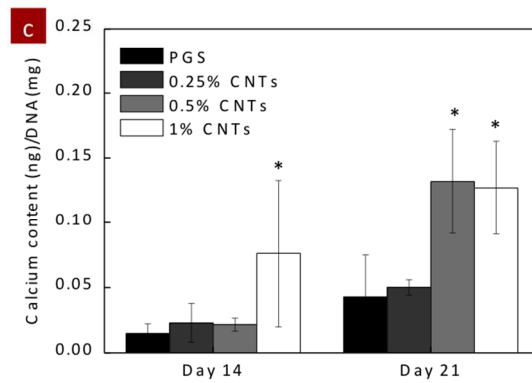
246x527mm (72 x 72 DPI)

PGS-CNTs Nanocomposites – As prepared

PGS-CNTs Nanocomposites – After mechanical deformation

650x392mm (72 x 72 DPI)